Analytical Methods

Accepted Manuscript

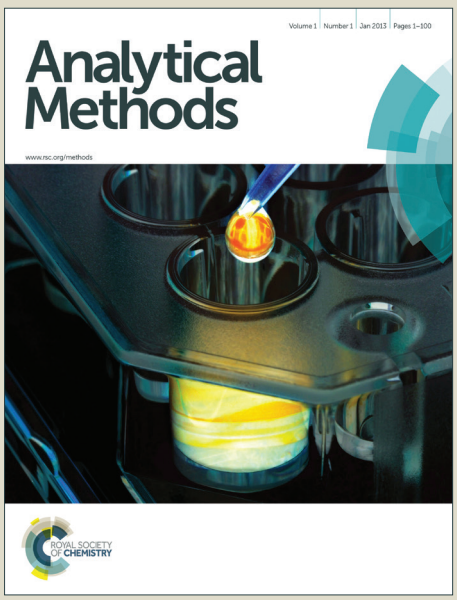

ROYAL SOCIETY OF CHEMISTRY

www.rsc.org/methods

Selective determination of dopamine and uric acid using electrochemical sensor based on poly (alizarin yellow R) film modified electrode

Yuanzhen Zhou *, Weimin Tang, Jing Wang, Guo Zhang, Shouning Chai, Liang Zhang, Ting Liu

School of science, Xi'an University of Architecture and Technology, Xi'an, 710055, China

* Corresponding author at: School of science, Xi'an University of Architecture and Technology, No. 13, Yanta Road, Xi'an, Shaanxi Province, 710055, China.

Tel.: +86 29 82201498 8619; fax: +86 29 82201498 8619.

E-mail address: zyz1289@126.com; zhouyuanzhen@xauat.edu.cn (Y. Zhou)

Abstract A sensitive and selective method based on poly (alizarin yellow R) modified carbon paste electrode (PAYR/CPE) to detect dopamine (DA) and uric acid (UA) was successfully established. The morphologies of the electrode surface were observed by scanning electron microscopy (SEM). Electrochemical characterization of the PAYR/CPE was investigated by electrochemical impedance spectroscopy (EIS), cyclic voltammetry (CV) and differential pulse voltammetry (DPV). It was illustrated that the PAYR/CPE had excellent electro-catalytic ability toward the oxidation of DA. The anodic peak current of DA was greatly enhanced at the PAYR/CPE and the standard rate constant (k_s) could be calculated to be 6.17 s^{-1}. The linear calibration curves are obtained as 0.49-70.1 μM and 83.6-488.14 μM for DA and 27.8-304.4 μM and 381.6-1117.9 μM for UA by DPV. The detection limits are 0.16 μM for DA and 9.5 μM for UA. Moreover, the modified electrode was applied to the selective detection of DA and UA with high sensitivity and selectivity. Furthermore, the modified electrode displayed high reproducibility and stability for these species determination. Thus, the proposed electrode could be conveniently employed for the determination of DA and UA in real samples and shown satisfactory results.

Keywords: Alizarin yellow R; Dopamine; Uric acid; Selective determination.

1. Introduction

Dopamine (DA) is a crucial neurotransmitter in the mammalian central nervous system (CNS). The cerebral dopaminergic system is implicated in the pathophysiology of several neurobehavioral disorders, such as Parkinson′s disease, hyperactivity disorders, schizophrenia, depression, substance abuse and eating disorders.[1] DA makes important contribution to the neurophysiological control of arousal and attention, initiation of movement, perception, motivation, and emotion.[2] Uric acid (UA) is an important final product of purine in the human metabolism. The abnormal level of UA has resulted in kidney, lesch-nyan disease, gout and hyperuricemia disorders in the human beings.[3-4] Therefore, both of them are play significant roles in human health and it is vitally important to selective determine the content of DA and UA in the clinical and pathological research.

At present, various analytical techniques have been used for determination of DA and UA, including mass spectrometry,[5] spectrophotometry,[6] fluorescence[7] and other method. While these methods require sophisticated and expensive instruments, electrochemical measurement[8-9] can make up those shortages due to their advantages of rapid, simple operation, easy to apply, sensitivity and real-time monitor analytes in low concentrations. Ascorbic acid (AA) also exists in human body fluids with high concentrations and can be easily oxidized at potential that close to DA and UA. Therefore, its presences interfere with the determination of DA and UA.[10-11] Chemically modified electrodes (CMEs) can solve these problems because of their characteristics such as easier fabrication process, more excellent electrochemical catalysis ability and physical stability. Various materials have been used for assemble CMEs to detect DA and UA. Chitravathi et al.[12] have used poly (naphthol green B)-film modified carbon paste electrode (CPE) to

determine DA and UA. Zhu et al.[13] reported that detecting DA based on hollow gold nanoparticles-graphene composite modified electrode. Qian et al.[14] have fabricated situ polymerization of highly dispersed polypyrrole on reduced graphite oxide for DA detection. Zen et al.[15] have developed clay-modified electrodes for UA and DA detection. Above examples shown that active materials are very important to CMEs. Hence, it is significant to look for new and appropriate materials to efficiently and expediently detect DA and UA.

Alizarin Yellow R (AYR), one of azo dyes with a salicylic acid structure (shown in Scheme. 1). This reagent was able to collect some metal ions effectively on a membrane filter from an aqueous solution by filtration under suction.[16] Occasionally it is used as a pH indicator[17] and rarely as the modified material for electrochemical sensor. Recently, Zhang and his co-worker[18] used AYR with silver nanoparticles as a modifier for the fabrication of hydrogen peroxide (HP) sensor. Wang and his co-worker[19] fabricated a poly (alizarin yellow R) modified glassy carbon electrode (PAYR/GCE) and appliede it for electrocatalysis of UA.

In this work, PAYR/CPE as a biosensor was fabricated by electropolymerization method. Cyclic voltammetry (CV) and differential pulse voltammetry (DPV) was applied to research the electrochemical response to DA and UA at proposed sensor. Subsequently, the effect of pH and scan rate on the electrochemical behavior of DA has been considered in detail. These sensors allow for better sensitivity and selectivity for the determination of DA in the presence of UA compared with bare electrode. In addition, interferes from AA and other substances were investigated. Finally, the biosensor was used for the determination of DA and UA in pharmaceutical and urine samples.

Scheme. 1

2. Experimental

2.1 Reagents and stock solutions

Graphite powder and paraffin were purchased from Sinopharm Chemical Reagent Company (China). Dopamine hydrochloride injection was purchased from Shanghai HeFeng Pharmaceutical Co. Ltd. China. AA and UA were obtained from China National Medicine Corporation. Alizarin yellow R was purchased from Aladdin Chemistry Co. Ltd. China. $K_3Fe(CN)_6$, $K_4Fe(CN)_6$, KCl, Na_2HPO_4, NaH_2PO_4, H_3PO_4, NaOH were obtained from China National Medicine Corporation. All the chemicals were of analytical reagent grade and used without further purification. 0.1 M phosphate buffer solutions (PBS) with different pH values (from 2.0 to 9.0) were prepared by mixing the stock solutions of Na_2HPO_4 and NaH_2PO_4, and adjusting the pH with H_3PO_4 or NaOH. All solutions were prepared with double distilled water.

2.2 Apparatus

All electrochemical experiments were carried out using a CHI 660 D electrochemical workstation (Chenhua Instruments in Shanghai, China). A conventional three-electrode system was used, where a modified and bare CPE (carbon paste electrode) as the working electrode, a platinum wire and SCE (saturated calomel electrode) as the counter electrode and the reference electrode, respectively. Adjustment of pH was carried out using a Mettler Toledo Delta 320pH meter (Shanghai, China). The surface morphology of the sensor was analyzed by scanning electron microscope (SEM, Quanta 200). All the electrochemical experiments were carried out at room temperature of 25±0.2℃.

2.3 Preparation of the modified electrodes

The CPE was prepared via mix graphite powder and mineral oil at the ratio of 5:0.7 (w/w) in a mortar and then pack the mixture into an insulating tube (3 mm diameter; 3 cm depth) carefully. Electrical contact was established with a copper wire. The CPE surface was mechanically polished against weighing paper and rinsed with double distilled water. Then, the poly-alizarin yellow R was electrochemically deposited on the surface of CPE by cyclic sweeping from -1.8 to 2.0 V at scan rate of 100 mV s^{-1} for 11 cyclic times in 0.1 M PBS (pH 9.5) containing 0.06 mM alizarin yellow R (All the electrochemical polymerization conditions such as pH, potential, scan rate and scaning cycles were optimized by CV). After electrochemical polymerization of alizarin yellow R and each measurement, the modified electrode was rinsed with doubly distilled water, and then treated in pH 7.0 PBS by repetitive scanning in the potential range of -0.4 V to 0.8 V at a scan rate of 100 mV s^{-1} until a stable blank background was obtained. The electrode was then stored at room temperature.

2.4 Electrochemical measurements

A standard three-electrode system connected to the CHI 660 D was used for electrochemical measurements. EIS measurements were carried out in 5.0 mM $K_3Fe(CN)_6/K_4Fe(CN)_6$ (1:1) mixture containing 0.1 M KCl, while the applied perturbation amplitude was 0.005 V, the frequencies swept from 50 mHz to 100 kHz. CV measurements were recorded by cycling the potential between -0.4 V and 0.8 V at a scan rate of 100 mV s^{-1} and the optimum accumulation time of 40s for DA. DPV measurements were performed from -0.2 to 0.6 V or -0.2 to 0.8 V at pulse amplitude of 0.05 V. PAYR/CPE could be used repeatedly after rinsed with double distilled water. All the experiments were carried out at room temperature.

3. Results and discussion

3.1 Electropolymerization of alizarin yellow R on the CPE surface

Electrochemical polymerization on the CPE surface was carried out using 0.06 mM AYR aqueous solution in 0.1 M PBS (pH 9.5) by applying potential cycling between -1.8 and 2.0 V at the scan rate of 100 mV s^{-1}. The cyclic voltammogram during the electropolymerization process up to the 11th cycle is shown in Fig. 1. As shown in this figure, it is clear that a broad cathodic peak at -0.52 V corresponding to the reduction of alizarin yellow R increased gradually with cyclic time increasing. The peak current was getting larger and larger with the successive scanning, reflecting the continuous growth of the film. The redox peaks increase as the number of cycles increases, indicating additional electroactive PAYR film deposition for each cycle. During the process of electropolymerization, the redox process corresponds to the electron transfer from solution to the electrodeposited PAYR film. This phenomenon indicated that PAYR film was successfully deposited on the surface of CPE.

Fig. 1

3.2 Characterization of surface morphology modified CPE with PAYR

In order to observe the differences of surface morphologies between bare CPE and PAYR/CPE, Fig. 2 shows the SEM images of the different electrode surface. According to Fig. 2A, the surface of bare CPE was irregularly shaped flakes of graphite, exhibiting a rough and black surface. However, after the PAYR film was successfully electro-polymerized on the surface of bare CPE (Fig 2B), obtaining a very smooth surface and covered with dense and fine film. The obvious differences on the surface morphologies confirmed that the CPE was coated by PAYR

film.

Fig. 2

3.3 Electrochemical impedance characterization of modified electrodes

Fig. 3A shows the cyclic voltammetric responses of bare CPE (a) and PAYR/CPE (b) in the 5.0 mM $K_3Fe(CN)_6/K_4Fe(CN)_6$ (1:1) solution with 0.1 M KCl as the supporting electrolyte. The peak current increased dramatically and a decrease in the peak-to-peak separation between the cathodic and anodic waves are clearly visible when the PAYR film was modified on the surface of bare CPE. The results of the CV demonstrate that the PAYR film is conductive and does not block electron transfer, which indicated that PAYR/CPE could greatly increase the electron transfer rate of $[Fe(CN)_6]^{3-/4-}$. Electrochemical impedance spectroscopy (EIS) was carried out to further study the characterization of the modified electrode and clarify the electrochemical performance differences among bare CPE and PAYR/CPE. EIS can provide useful information on the impedance changes of the modified electrode surface.[20-21] And it is also a powerful tool for probing the features of surface-modified electrode, the semicircle diameter of EIS equals to the electron transfer resistance (R_{ct}). This resistance controls the electron transfer kinetics of the redox-probe at electrode interface. Fig. 3B shows Nyquist plots of 5.0 mM $K_3Fe(CN)_6/K_4Fe(CN)_6$ (1:1) probe in 0.1M KCl at different electrodes. As curve a) showed, a large diameter was observed for the bar CPE in 78 kΩ. However, the diameter of the semicircle diminished when PAYR/CPE were employed. Curve b) showed an arc, the diameter of which displayed R_{ct} = 4.0 kΩ. The Nyquist diameter of the PAYR/CPE is much smaller than that of the bare CPE, which suggests that the PAYR film coated on the CPE can further accelerate the electron transfer of the redox probe.

Fig. 3

3.4 Electrochemical behavior of DA

The PAYR/CPE shows excellent electro-catalysis activities towards the oxidation of DA. Fig. 4 shows the cyclic voltammograms of DA in pH 7.0 PBS at a bare CPE (curve a) and PAYR/CPE (curve b). At bare CPE, a weak oxidation peak at 0.4 V was observed and almost no reduction peak exhibited. While a couple of well-defined redox peak is obtained at PAYR/CPE, accompanied with a six-fold enhanced I_{pa}. The anodic peak potential (E_{pa}) shifted negatively to 0.170 V and cathodic peak (E_{pc}) appeared at 0.132 V, which resulted in a well-defined redox peak of DA with the separation of peak potentials separation ($\Delta E_p = E_{pa} - E_{pc}$) as 0.038 V. Greatly enhanced peak current and smaller peak separation strongly indicated excellent catalysis ability of PAYR film and the faster electron transfer of DA. This suggested that the PAYR/CPE shows a good electrochemical oxidation towards DA.

Fig. 4

3.5 Influence of pH

As protons take part in the electrochemical oxidation process of DA,[12, 22] the pH of solution is a significant factor to influence the electrochemical reaction of DA. Thus, it is important to investigate the effect of solution pH on electrochemical behavior of DA at PAYR/CPE. As shown in Fig. 5, CV was carried out to characterize the effect of different solution pH value. It was found that peak potential shifted negatively with the increase of solution pH, indicating that the electrocatalytic oxidation of DA at the PAYR/CPE is a pH-dependent reaction. The relationship of E_{pa} and E_{pc} with pH could be described by the following linear regression equation: E_{pa} (V) =

0.568 – 0.0566 pH (r = 0.9933), E_{pc} (V) = 0.511 – 0.0547 pH (r = 0.9979) (inset of Fig. 5). The slope was found to be -56.6 mV pH^{-1} and -54.7 mV pH^{-1} over the pH range from 2.0 to 9.0, which is very close to the theoretical value of -59 mV pH^{-1}, proving that the electrode process is two-proton coupled with two-electron transfer.[23] Due to the pH value of human blood and urine is close to 7, pH 7.0 is chosen as the optimum pH value for their determination.

Fig. 5

3.6 Influence of scan rate

The influence of scan rates on the electrochemical behavior of DA at PAYR/CPE was also investigated by CV method and shown in Fig 6. Both the peak potential (E_p) and peak current (I_p) are affected by scan rate. The anodic and cathodic peak currents of DA at PAYR/CPE increased linearly with the scan rate increasing from 20 to 600 mV s^{-1}. In order to confirm that the process was controlled by diffusion or adsorption, the relationship of logarithm of peak current (log I_p) versus logarithm of scan rate (log v) was discussed (Fig 6 inset a). Relevant literatures indicated that the electro-catalysis of DA was greatly involved with the slope value of log I_p-log v.[24] The slope between 0.5 and 1.0 suggests that the process is simultaneously controlled by the diffusion and the adsorption. The slopes of 0.5 and 1.0 indicate that the electrode reaction is severally controlled by the diffusion and the adsorption, respectively. For 50 μM DA in pH 7.0 PBS, the log I_p-log v showed linear relationship with the regression equations of log I_{pa} (A) = 1.0296 + 0.6098 log v (V s^{-1}) (r =0.9979), and log I_{pc} (A) = 0.9975 + 0.8073 log v (V s^{-1}) (r = 0.9979), respectively, which indicates that both the oxidation process and reduction process were controlled by diffusion accompanied with adsorption.

The relationship of peak potential (E_p) and log v was also discussed, as shown in Fig 6 inset b.

All over the scan process, the oxidation peak potential (E_{pa}) shifted to the positive direction and the reduction peak potential (E_{pc}) to the negative direction with the increase of scan rate. The values of peak potential almost have no change at low scan rate (20-400 mV s^{-1}). However, the value of peak potential increased linearly with the scan rate increasing from 500 to 1900 mV s^{-1}. The relationships between E_p and log v were established with the results shown in inset Fig. 6b. The regression equations were calculated as E_{pa} = 0.1982 + 0.6098 log v (r = 0.9942) and E_{pc} = 0.1114 – 0.0605 log v (r = 0.9984). Hence, according to Laviron theories: [25]

$$E_{pc} = E^{0'} - \frac{2.3RT}{\alpha nF}\log v \quad (1)$$

$$E_{pa} = E^{0'} + \frac{2.3RT}{(1-\alpha)nF}\log v \quad (2)$$

$$\log k_s = \alpha\log(1-\alpha) + (1-\alpha)\log\alpha - \log\frac{RT}{nFv} - \frac{(1-\alpha)\alpha nF\Delta E_p}{2.3RT} \quad (3)$$

Where n is the number of electron transferred, F is the Faraday's constant, v is the scan rate. From the slopes of the equations (1) and (2) the charge transfer coefficient (α) and the number of electron transferred (n) can be calculated as 0.49 and 1.979 ≈ 2, respectively. The value indicates that two electron are involved in the reaction for DA at the PAYR/CPE and the process is shown in Scheme 2. While v = 1500 mV s^{-1}, ΔE_p=116 mV, and then $n\Delta E_p$>200 mV. The electron transfer rate constant (k_s) for oxidation process could be calculated as 6.17 s^{-1} according to equations (3), indicating that PAYR has prominent catalysis ability for the redox reaction of DA at the electrode.

Fig. 6

Scheme 2

3.7 Determination of DA and UA

Differential pulse voltammetric (DPV) was used here to detect DA and UA, because it has much higher current sensitivity and better resolution than cyclic voltammetry. The DPV responses of different concentration of DA and UA at the PAYR/CPE were recorded in Fig. 7A and B. As clearly show in inset of Fig. 7A, the plot of peak current versus DA concentration displayed linear relationship in two segments as: I_{pa} (μA) = 0.3797 + 0.0712 c (μM) (r = 0.9911, 0.49~70.1μM), and I_{pa} (μA) = 4.0120 + 0.0147 c (μM) (r = 0.9989, 83.6~488.14 μM), respectively. The slope variation for the two regions may be an evidence of mechanism change for DA transport from solution toward the electrode surface, which could be described as adsorptive mode and diffusion controlled process for the lower and higher regions of DA concentration.[26] The detection limit (LOD) is found to be 0.16 μM for DA based on the signal-to-noise ratio of 3 (3S/N). Furthermore, Fig. 7B illustrates the DPV responses of PAYR/CPE toward various UA concentrations. From the figure, it can be seen that the peak current exhibits linear increase with the increased concentration of UA, obtaining a linear function of I_{pa} (μA) = 0.0930 + 0.0105 c (μM) (r = 0.9947, 27.8~304.4μM) and I_{pa} (μA) = 2.3031 + 0.0036 c (μM) (r = 0.9974, 381.6~1117.9 μM), respectively. Besides, the detection limit for UA is 9.5 μM. Table 1 summarized the linear range and detection limits for DA and UA of this proposed method compared with other existing methods with different modifiers. The results show that the electrochemical polymerization of AYR on the CPE surface can enhance the analytical characteristics of DA.

Fig. 7

Table 1

3.8 Selective determination of DA and UA

The individual determination of DA or UA in their mixtures was performed at PAYR/CPE

with the concentration of one species changed and the other species remained constant. Fig. 8A shows DPV curves of different concentrations of DA in pH 7.0 PBS coexisting 0.1 mM UA. The results showed that peak current of DA ($I_{pa,\ DA}$) was proportional to its concentration, while the oxidation peak current for UA keeps nearly unchanged. The regression equations are $I_{pa,\ DA}$ (μA) = 0.0731 + 0.1331 c_{DA} (μM) (0.33~13.1 μM) and $I_{pa,\ DA}$ (μA) = 0.5723 + 0.0715 c_{DA} (μM) (16.49~49.3 μM) with linear relative coefficient r = 0.9939 and 0.9973, respectively. Similarly, as shown in Fig. 8B, remaining the concentration of DA unchanged, the anodic peak current of UA ($I_{pa,\ UA}$) increased linearly with the concentration of UA and without obvious influence on the peak response of DA. Linear equations are expressed as $I_{pa,\ UA}$ (μA) = 0.0193 + 0.5591 c_{UA} (μM) (r = 0.9960, 4~404 μM) and $I_{pa,\ UA}$ (μA) = 1.6836 + 0.1772 c_{UA} (μM) (r = 0.9923, 474~1300 μM), respectively. The results indicate that the responses to DA and UA at the PAYR/CPE are comparatively independent.

Fig. 8

3.9 Interference study

DA, UA and AA coexist in human body fluid and they are all oxidized at nearly the same potential, which usually make their electrochemical signal overlap. Interference from AA and UA was investigated in this paper. Fig 9 shown the CV of (a) 0.5 mM AA, (b) 0.25 mM UA, (c) 50 μM DA, (d) 0.5 mM AA + 0.25 mM UA + 50 μM DA in 0.1 M PBS (pH 7.0) at PAYR/CPE. As shown in curve a), no obvious anodic peak of AA was obtained. However, DA and UA shows well defined anodic peaks at 170 and 300 mV as depicted in curve b) and c), respectively. While mixed this three species together, the peak potential to DA and UA (curve d) almost have no change. The results indicated that AA does not influence the oxidation process of DA and UA

even the concentration of AA is 10 times higher than those of DA. In addition, other possible interfering substances were also studied by above process including glucose (200), citric acid (100), tartaric acid (100), lysine (Lys, 200), tyrosine (Try, 200), NaCl (500), KCl (500), $CaCl_2$ (500) and $ZnCl_2$ (500) for the detection of DA and UA, respectively. The results indicated that the determination of DA and UA was insignificantly affected by the most common interfering species at PAYR/CPE.

Fig. 9

3.10 Reproducibility and stability

Stability and repetitive measurements were carried out in 50 μM DA solutions to characterize the reproducibility of PAYR/CPE by monitoring the CV peak currents. The results of 20 times successive measurements shown in Fig 10 and the relative standard deviation (RSD) of 3.0%, indicating that the electrode has a remarkable reproducibility. When the sensor was stored in atmosphere at room temperature and measured at interval of seven days. It retained about 95% of its original activity after seven days. The results prove that the stability of this modified electrode is relatively satisfactory.

Fig. 10

3.11 Determination of DA and UA in real samples

The practical application of PAYR/CPE was tested by detecting the concentration of DA and UA using the standard addition method. Dopamine hydrochloride injection as real samples were purchased in local pharmacy. And human urine samples were provided by our own member of this project team for analysis. All samples were diluted with 0.1 M PBS (pH 7.0). First, dopamine

hydrochloride injection solution (concentration of DA 10 mg mL^{-1}, 2.0 mL per injection) was diluted to 5.30 μM with PBS. Then added the different concentrations of DA standard solution in test solution and placed in an electrochemical cell to detect DA using the above DPV method.

The modified electrode was also investigated by a direct analysis of UA in human urine samples. All the urine samples used for detection were diluted by 100 times with PBS before measurement. The recoveries were 100.07%, 100.06% and 99.36%, respectively. The results of all analysis are summarized in Table 2. The proposed method showed a better recovery of spiked DA and UA suggesting that the proposed method could be used for the determination of DA and UA in real samples.

Table 2

4. Conclusions

In conclusion, the sensor based on PAYR/CPE was prepared by simply electropolymerization. The catalysis activity of modified CPE towards DA and UA was improved by the formation of a uniform PAYR film on the electrode surface. In addition, the sensor exhibits good selectivity toward the determination of DA and UA. The electro-catalysis currents increase linearly with DA and UA concentrations rang in 0.49-488.14 μM and 27.8-1117.9 μM by DPV method, with the detection limits of 0.16 μM and 9.5 μM, respectively. With the excellent features such as wide linear dynamic range, high sensitivity and selectivity as mentioned above, the sensor provides a new strategy for the determination of DA and UA in real samples and exhibiting satisfactory results.

Acknowledgements

This work was supported by the Basic Research Foundation (No. JC1014), the Youth

Scientist Foundation of Xi'an University of Architecture & Technology (No. RC0942), the National Natural Science Foundation of China (No. 21205092) and the Shaanxi Provincial Education Department Foundation (No. 2013JK0652).

References

[1]. A. Heinz, H. Przuntek, G. Winterer, A. Pietzcker, *Nervenarzt*, 1995, **66**, 662-669.

[2]. A. Zhang, J.L. Neumeyer, R.J. Baldessarini, *Chem. Rev.*, 2007, **107**, 274-302.

[3]. T.H. Tsai, S. Thiagarajan, S.M. Chen, C.Y. Cheng, *Thin Solid Films*, 2012, **520**, 3054-3059.

[4]. J.P. Dong, Y.Y. Hu, S.M. Zhu, J.Q. Xu, Y.J. Xu, *Anal. Bioanal. Chem.*, 2010, **396**, 1755-1762.

[5]. K.Vuorensola, H. Sirén, U. Karjalainen, *J. Chromatogr. B.*, 2003, **788**, 277-289.

[6]. M.R. Moghadam, S. Dadfarnia, A.M.H. Shabani, P. Shahbazikhah, *Anal. Biochem.*, 2011, **410**, 289-295.

[7]. D.P. Nikolelis, D.A. Drivelos, M.G. Simantiraki, S Koinis, *Anal. Chem.*, 2004, **76**, 2174-2180.

[8]. R. Salgado, R. del Rio, M.A. del Valle, F. Armijo, *J. Electroanal. Chem.*, 2013, **704**, 130-136.

[9]. E. de Pieri Troiani, R.C. Faria, *J. Appl. Electrochem.*, 2013, **43**, 919-926.

[10]. Z.H. Wang, J. Tang, F.F. Zhang, J.F. Xia, N. Sun, G.Y. Shi, Y.Z. Xia, L.H. Xia, L.C. Qin, *Int. J. Electrochem. Sci.*, 2013, **8**, 9967-9976.

[11]. S.F. Hou, M.L. Kasner, S.J. Su, K. Patel, R. Cuellari, *J. Phys. Chem. C.*, 2010, **114**, 14915-14921.

[12]. S. Chitravathi, B.E. Kumara Swamy, G.P. Mamatha, B.S. Sherigara, *J. Electroanal. Chem.*, 2012, **667**, 66-75.

[13]. W.C. Zhu, T. Chen, X.M. Ma, H.Y. Ma, S.H. Chen, *Colloids. Surf. B. Biointerfaces.*, 2013, **111**, 321-326.

[14]. T. Qian,C.F. Yu, S.S. Wu, J. Shen, *Biosens. Bioelectron.*, 2013, **50**, 157-160.

[15]. J.M. Zen, P.J. Chen, *Anal. Chem.*, 1997, **69**, 5087-5093.

[16]. K. Ihara, S.I. Hasegawa, K. Naito, *Talanta*, 2008, **75**, 944-949.

[17]. T.R. Williams, M. Lautenschleger, *Talanta*, 1963, **10**, 804-808.

[18]. K.Y. Zhang, N. Zhang, L. Zhang, J.G. Xu, H.Y. Wang, C. Wang, T. Geng, *Microchim. Acta.*, 2011, **173**, 135-141.

[19]. D.Y. Wang, N. Zhang, K.Y. Zhang, B.H. Huang, *Chinese Journal of Analysis Laboratory*, 2012, **31**, 113-115.

[20]. S.S. Jia, J.J. Fei, J.J. Deng, Y.L. Cai, J.N. Li, *Sens. Actuators. B. Chem.*, 2009, **138**, 244-250.

[21]. M. Zheng, Y. Zhou, Y. Chen, Y.W. Tang, T.H. Lu, *Electrochimica. Acta.*, 2010, **55**, 4789-4798.

[22]. Z.J. Yang, X.C. Huang, J. Li, Y.C. Zhang, S.H. Yu, Q. Xu, X.Y. Hu, *Microchim. Acta.*, 2012, **177**, 381-387.

[23]. S.J. Li, D.H. Deng, Q. Shi, S.R. Liu, *Microchim. Acta.*, 2012, **177**, 325-331.

[24]. W. Ma, D.M. Sun, *Chin. J. Anal. Chem.*, 2007, **35**, 66-70.

[25]. E. Laviron, *J. Electroanal. Chem.*, 1979, **101**, 19-28.

[26]. Y.Z. Zhou., H.Y. Zhang, J. Zhang, T. Liu, W.M. Tang, *Sens. Actuators. B. Chem.*, 2013, **182**, 610-617.

[27]. E. de Pieri Troiani, R. C. Faria, *J. Appl. Electrochem.*, 2013, **43**, 919-926.

[28]. S. Thiagarajan, S.M. Chen, *Talanta*, 2007, **74**, 212-222.

[29]. M. Mazloum-Ardakani, M.A. Sheikh-Mohseni, A.Benvidi, *Electroanalysis*, 2011, **23**, 2822-2831.

[30]. D. Didem, H. Erdogan, O.S. Ali, Curr. *Anal. Chem.*, 2010, **6**, 203-208.

[31]. Ali A. Ensafi, M. Taei, T. Khayamian, *J. Electroanal. Chem.*, 2009, **633**, 212-220.

Figure captions

Fig. 1 Displays the continuous CVs for the electrochemical polymerization of alizarin yellow R over the range of -1.8 to 2.0 V at 100 mV s^{-1} for 11 cycles.

Fig. 2 SEM image of (A) bare CPE and (B) PAYR/CPE.

Fig. 3 (A) CVs and (B) EIS on (a) bare CPE and (b) PAYR/CPE. CVs were recorded in 5.0 mM $K_3[Fe(CN)_6]/K_4[Fe(CN)_6]$ (1:1) mixture containing 0.1 M KCl at a scan rate of 100 mV s^{-1}; EIS was obtained in 5.0 mM $K_3[Fe(CN)_6]/K_4[Fe(CN)_6]$ (1:1) mixture containing 0.1 M KCl and the applied perturbation amplitude was 0.005 V.

Fig. 4 CVs of 50 μM DA at: bare CPE (a) and PAYR/CPE (b) in 0.1 M PBS (pH 7.0) with the scan rate of 100 mV s^{-1}.

Fig. 5 CVs of 50 μM DA at the PAYR/CPE in different pHs: (a) 2.0, (b) 3.0, (c) 4.0, (d) 5.0, (e) 6.0, (f) 7.0, (g) 8.0, and (h) 9.0 (from left to right). Inset: the plots of effects of pH on the anodic peak potentials at the PAYR/CPE.

Fig. 6 CVs of the PAYR/CPE in the presence of 50 μM DA with varying scan rate. CVs were measured in 0.1 M PBS (pH 7.0). Scan rate (V s^{-1}): 0.02, 0.08, 0.15, 0.24, 0.32, 0.40, 0.50, 0.60, 0.75, 0.90, 1.00, 1.10, 1.20, 1.30, 1.40, 1.50, 1.60, 1.70, 1.80, 1.90 (1→20). Inset a): shows a linear relationship between the logarithm of the peak currents versus logarithm of scan rate. b) The relationship of the peak potential E_p against log ν.

Fig. 7 (A) DPVs of PAYR/CPE in 0.1 M PBS (pH 7.0) containing different concentrations of DA (from number 1→30): 0.49, 0.59, 0.89, 1.34, 2.04, 3.14, 4.64, 6.54, 8.84, 11.54, 14.64, 20.04, 24.14, 31.04, 36.14, 41.64, 47.84, 54.84, 62.64, 70.14, 83.64, 97.14, 114.14, 136.14, 166.14, 204.14, 253.14, 315.14, 393.14 and 488.14 μM; Inset shows the calibration curve of DA for

concentrations from 0.49 to 488.14 μM. (B) DPVs of the PAYR/CPE in 0.1 M PBS (pH 7.0) containing different concentrations of UA (from number 1→20): 27.8, 31.8, 41.6, 54.4, 70.4, 90.2, 114, 141.8, 174.2, 211.4, 254.6, 304.4, 381.6, 448.0, 525.6, 617.6, 727.2, 858.0, 1015.6 and 1117.9 μM; Inset shows the calibration curve of UA for concentrations from 27.8 to 1117.9 μM.

Fig. 8 (A) DPVs of PAYR/CPE in 0.1 M PBS (pH 7.0) containing different concentrations of DA in the presence of 0.1 mM UA (from number 1→28, inset a 1→11): 0.33, 0.45, 0.66, 0.84, 1.08, 1.44, 2.0, 2.84, 4.04, 4.80, 5.67, 6.65, 7.63, 8.83, 10.14, 11.56, 13.09, 16.49, 22.3, 24.5, 26.9, 29.5, 32.3, 35.3, 38.5, 41.9, 45.5 and 49.3 μM; Inset b: calibration plots of DA for concentrations from 0.33 to 49.3 μM. (B) DPVs of the PAYR/CPE in 0.1 M PBS (pH 7.0) containing different concentrations of UA in the presence of 5.0 μM DA (from number 1→25): 4.0, 12.3, 21.2, 31.0, 41.9, 54, 67.6, 83.0, 100.8, 121.2, 145, 173, 206, 244.8, 290.2, 343, 404, 474, 553.8, 644.2, 746, 860.6, 989.6, 1134.8 and 1300 μM; Inset shows the calibration curve of UA for concentrations from 4.0 to 1300.0 μM.

Fig. 9 CVs of (a) 0.5 mM AA, (b) 0.25 mM UA, (c) 50 μM DA, (d) 0.5 mM AA + 0.25 mM UA + 50 μM DA in 0.1 M PBS (pH 7.0) at PAYR/CPE; scan rate:100 mV s^{-1}.

Fig. 10 CVs of 50 μM DA at PAYR/CPE in 0.1 M PBS (pH 7.0) with 20 times successive measurements at scan rate of 100 mV s^{-1}

Table 1 The performance comparison of some modified electrodes for the determination of DA and UA at different modified electrodes.

Modified electrode	Detection limit (μM)		Linear range (μM)		References
	DA	UA	DA	UA	
Pt/PAAQ [a]	3.05	11.5	21.5-106	35-420	[27]
Au-Pt/GCE [b]	24	21	103-165	21-336	[28]
PPD/GCE [c]	1.0	2.5	10-1250	50-1600	[29]
I-3-CD/GCE [d]	1.7	4.99	10-100	10-100	[30]
PCCDA/GCE [e]	0.29	0.16	5.0-280	0.1-18	[31]
PAYR/CPE	0.16	9.5	0.49-70.1 83.6-488.14	27.8-304.4 381.6-1117.9	This work

[a] poly (1-aminoanthraquinone)-modified Pt disk electrode
[b] Au and Pt nanoparticles modified glassy carbon electrode
[c] para-phenylenediamine modified glassy carbon electrode
[d] Indole-3-Carboxaldehyde Modified Glassy Carbon Electrode
[e] poly (3-(5-chloro-2-hydroxyphenylazo)-4,5-dihydroxynaphthalene-2,7-disulfonic acid) film modified glassy carbon electrode

Table 2 Determination of DA and UA in real samples (n=3)

Sample	Original (μM)	Added (μM)	Found (μM)	Recovery (%)
Dopamine hydrochloride injection	5.30	5.00	10.21	99.16
	5.30	10.00	15.28	99.85
	5.30	15.00	20.39	100.37
Human urine	28.60	5.00	33.62	100.07
	28.60	10.00	38.65	100.06
	28.60	15.00	43.32	99.36

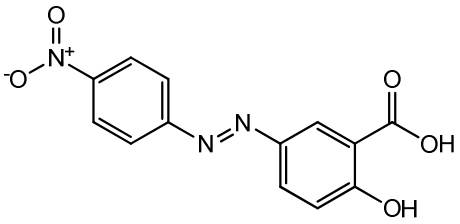

Scheme. 1. The molecular structure of alizarin yellow R

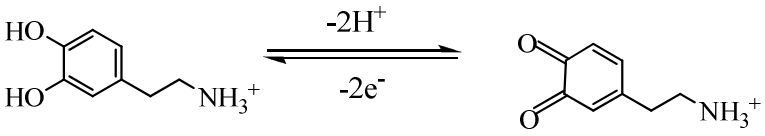

Scheme. 2. Oxidation mechanisms of DA

Fig.1

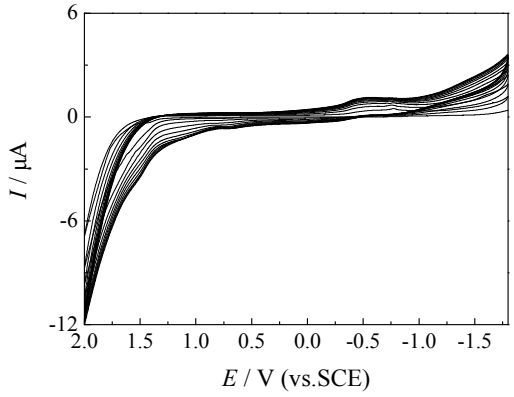

Fig.2A

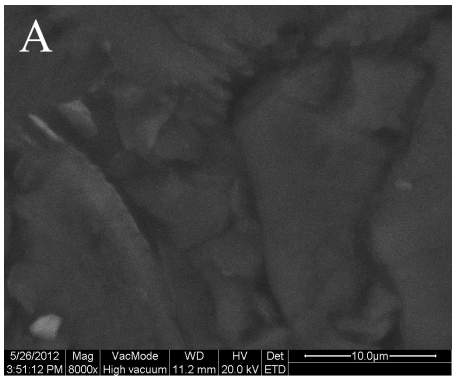

Fig.2B

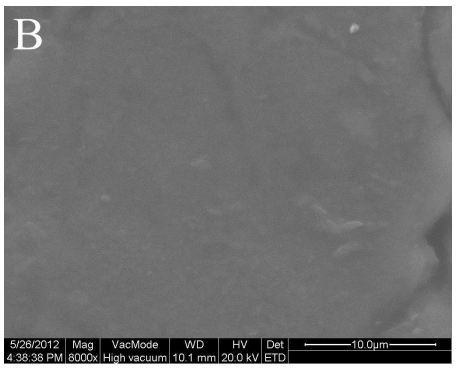

Fig.3A

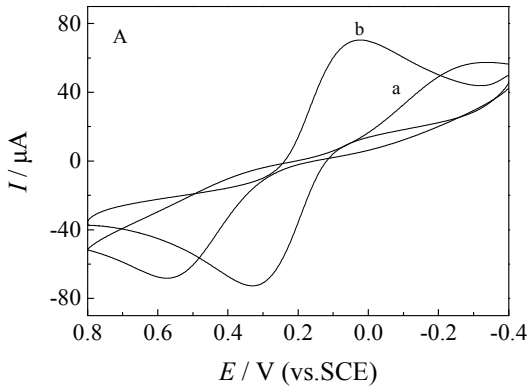

Fig.3B

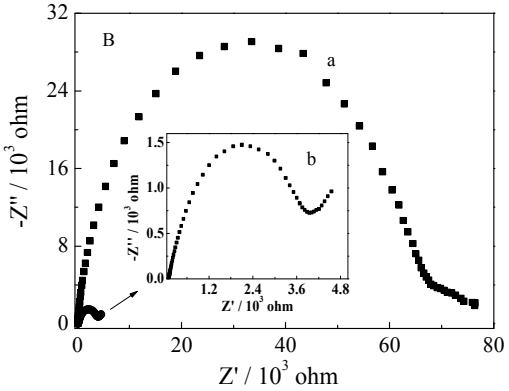

Fig.4

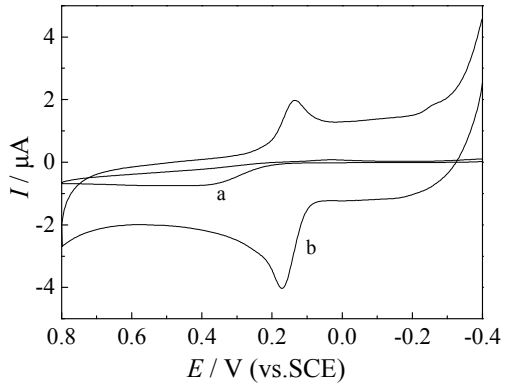

Fig.5

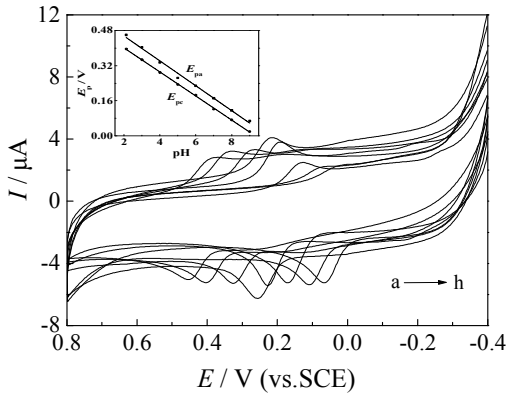

Fig.6

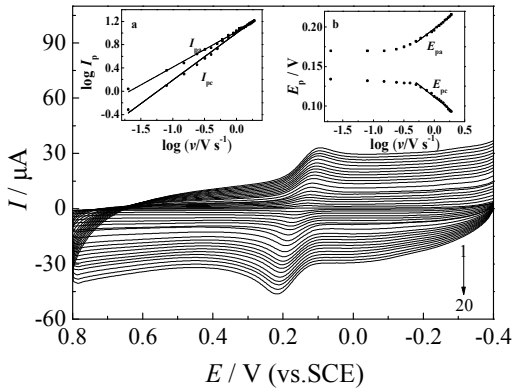

Fig.7A

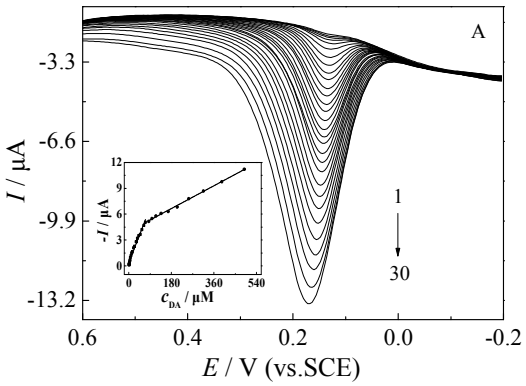

Fig.7B

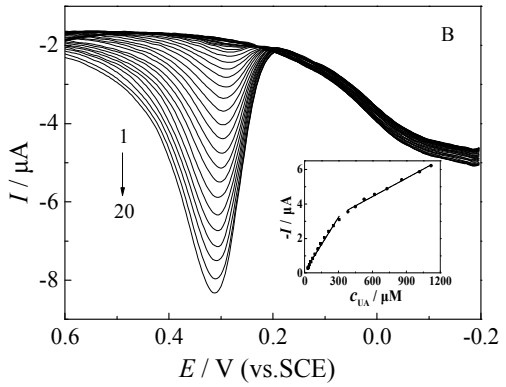

Fig.8A

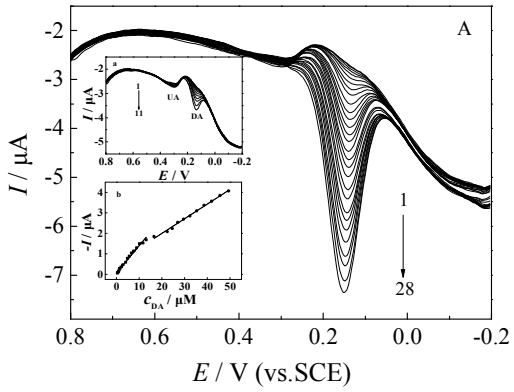

Fig.8B

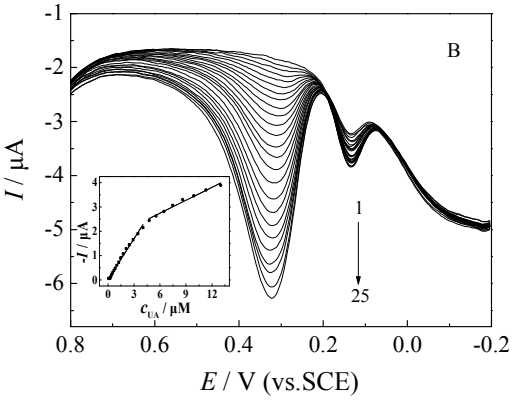

Fig.9

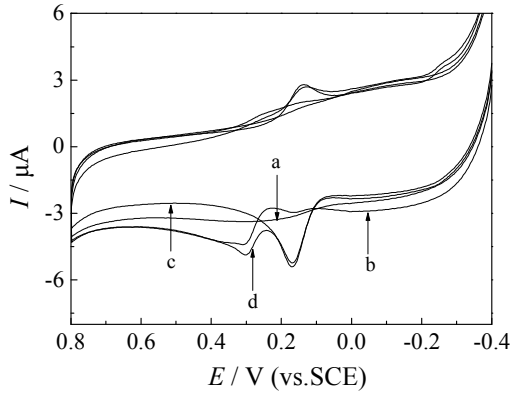

Fig.10